Influence of mode polarizations on the inelastic He-scattering spectrum: High-order commensurate Xe monolayer adsorbed on Cu(110)

C. Ramseyer, V. Pouthier, and C. Girardet*
Laboratoire de Physique Moléculaire, UMR CNRS 6624, Faculté des Sciences, La Bouloie, Université de Franche Comté, 25030 Besançon Cedex, France

P. Zeppenfeld, M. Büchel, V. Diercks, and G. Comsa
Institut für Grenzflächenforschung und Vakuumphysik, KFA-Forschungszentrum Jülich, D-52425 Jülich, Germany
(Received 10 June 1996)

The phonon dispersion curves for monolayer Xe adsorbed on Cu(110) were measured along the $\overline{\Gamma X}$ and $\overline{\Gamma Y}$ directions using inelastic He scattering. The dispersion along these two orthogonal high-symmetry directions is fundamentally different as a consequence of the substrate anisotropy. Coupled dynamics calculations using a slab model are performed on the square low-order commensurate $c(2\times2)$ structure and on the (26×2) high-order commensurate phase of the Xe monolayer, the latter being stable at low temperature. The calculations allow a quantitative interpretation of the hybridization and avoided crossings between the longitudinal and perpendicular monolayer branches and the Rayleigh mode along $\overline{\Gamma X}$. They can also account for the unexpected behavior of the monolayer longitudinal mode along $\overline{\Gamma Y}$, revealing a different type of dynamical coupling between this monolayer branch and the longitudinally polarized Rayleigh mode of the substrate. This coupling is responsible for a polarization exchange by which both modes become susceptible to He scattering detection. [S0163-1829(97)03319-5]

I. INTRODUCTION

Valuable information on the dynamical properties of surfaces is obtained from the investigation of the dispersion of surface phonons. Surface vibrations of a variety of metals and dielectrics have been experimentally studied[1] and it was shown that the surface phonon dispersion is quite different from what is expected from the mere truncation of the bulk solid. Detailed theoretical analyses[2] of the dispersion curves for clean surfaces have been performed using slab calculations or the Green's function formalism. In many cases, these methods have proven to be successful in interpreting the main experimental features. One of the difficulties encountered in the calculation of the dynamical matrix is the modification of the force constant values between crystal atoms in the vicinity of the surface. Tractable potential calculations are, in general, not accurate enough to account for the atomic and electronic redistribution in the surface region and to bring a reliable answer to this problem. As a way to work around this problem, semiempirical parameters describing the influence of the surface on the atom bonds are often used to quantify the changes of the surface force constants.

If, in addition, a monolayer is adsorbed on the substrate, the study of the dynamics of the whole system requires the knowledge of the monolayer-substrate interactions as well as the intralayer potentials.[3] Preliminary investigations of the equilibrium structure of the layer are necessary in order to conduct reasonable dynamical calculations. Most of the theoretical studies have been performed assuming the simplified scheme of either of two idealized situations. In the first case, an assumedly incommensurate monolayer is coupled to a quasiplanar substrate through a single force constant; as a result the entire dynamics is reduced to that of a floating monolayer coupled, through a perpendicular force constant, to a substrate which is approximated by an elastic continuum.[4] This model is appropriate for monolayers physisorbed on very smooth substrates. The second case applies to low-order commensurate monolayers with a limited number of atoms per unit cell. Slab[5] or Green's function[6] techniques are used to diagonalize the dynamical matrix and to determine the mode dispersion. However, as the size of the unit cell increases, by taking into account several inequivalent adsorption sites, the corresponding size of the dynamical matrix increases significantly and the dispersion curves display a much more intricate behavior including the energy gaps of quasiacoustic and quasioptic branches, the avoided crossings and the splittings due to the degeneracy removed by the non-commensurate overlayer.[7]

The Xe/Cu(110) system can be considered a model system for the richness of its structural phase diagram. Helium atom scattering experiments[8] show that high-order commensurate (HOC) structures containing up to 38 Xe atoms per unit cell appear to be stable for temperatures below 75 K. These HOC phases have ''centered'' $(n\times2)$ geometries (n integer) indicating that the Xe atoms are aligned along the smooth potential valleys along $[1\bar{1}0]$, i.e. parallel to the close packed Cu atomic rows. The much larger corrugation of the holding potential along the perpendicular [001] direction forces the Xe overlayer into perfect registry. Increasing the surface temperature up to 75 K leads to the sequential occurrence of HOC-HOC phase transitions which have been examinated by He atom diffraction.[9] At a low temperature, the (26×2) phase appears to be the most stable structure while the simple commensurate $c(2\times2)$ can be considered the limiting structure at high temperatures.[10] The two-dimensional (2D) unit cell of the (26×2) phase is repre-

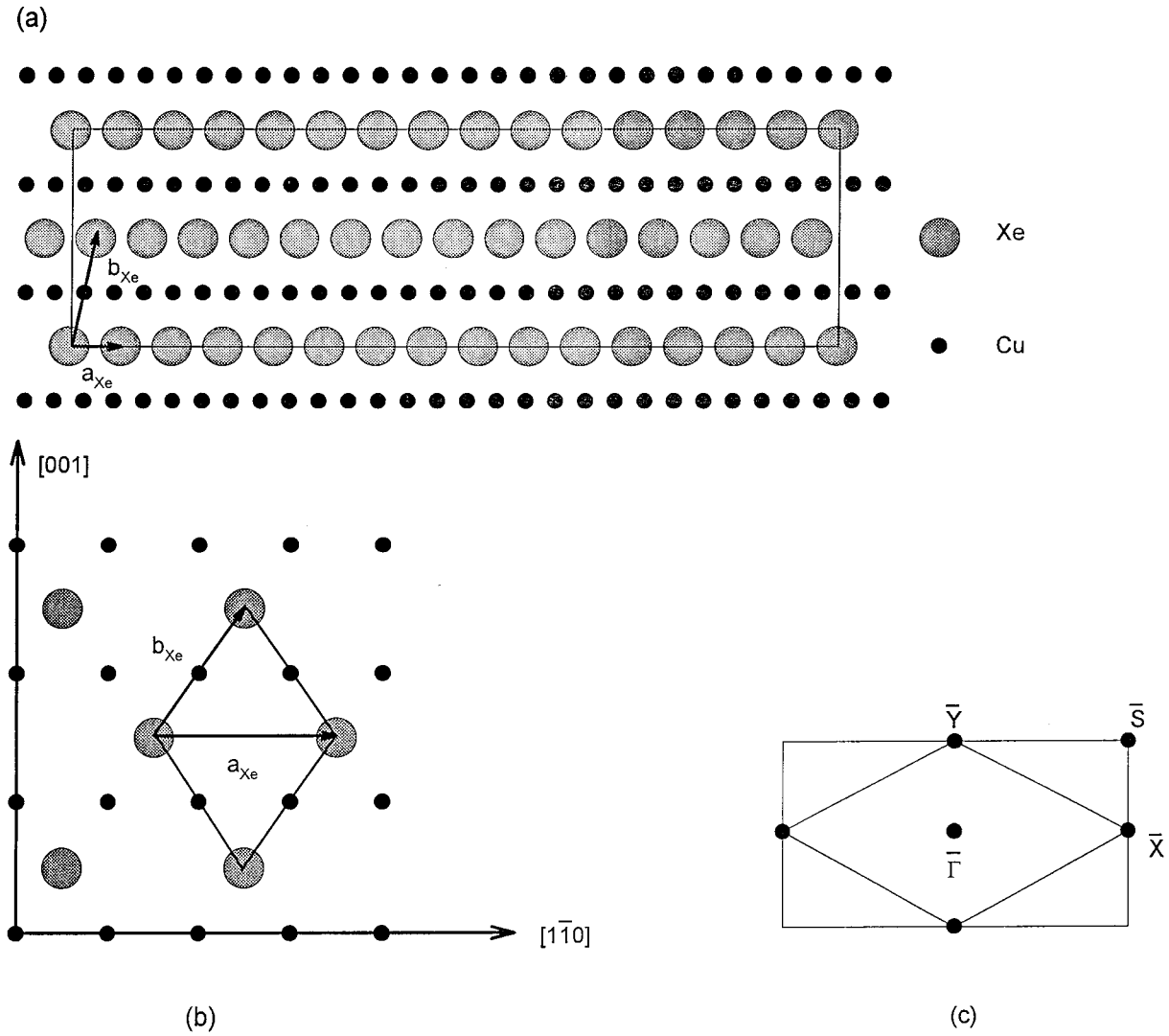

FIG. 1. Surface unit cells of the Xe monolayer on Cu(110): (26×2) phase (a) and $c(2\times2)$ phase (b). In (c) the first Brillouin zone of the Cu(110) substrate is shown together with the high-symmetry points. The reciprocal cell of the $c(2\times2)$ structure is indicated by the hatched area. By symmetry, for the $c(2\times2)$ structure $\bar{Y}\equiv\bar{X}$ and $\bar{\Gamma}\equiv\bar{S}$.

sented in Fig. 1(a). It contains 30 Xe atoms which are arranged in a quasihexagonal lattice, distorted by the anisotropic Cu surface. The overlayer is in perfect registry with the substrate along the [001] direction, while along the $[1\bar{1}0]$ direction, 15 Xe atoms cover 26 Cu lattice distances. The distance along the close packed $[1\bar{1}0]$ direction is $a_{Xe}=4.42$ Å and the distance between neighboring Xe atoms across the close packed Cu rows is $b_{Xe}=4.23$ Å. The lattice parameter for the ideal floating Xe monolayer is intermediate, about 4.36 Å. By contrast, the $c(2\times2)$ Xe phase contains one atom per unit cell [Fig. 1(b)] and has a lower density since the Xe interatomic spacings are $a_{Xe}=5.10$ Å and $b_{Xe}=4.42$ Å, respectively. Potential calculations[8] based on semiempirical parameters can quite well reproduce the sequence between the various HOC phases and they can accurately account for the values of the isosteric heat of adsorption for the Xe monolayer.

Inelastic helium atom scattering experiments are presented here for the most stable low temperature (26×2) phase and the dispersion curves are interpreted on the basis of the potentials already used to analyze the thermodynamic and structural data.[8,9] Different theoretical models are discussed. The one that takes into account the anisotropic distortion of the Xe monolayer in the (26×2) phase is shown to describe all the main experimental features. More specifically, the behavior of the monolayer vibrational modes can be explained in terms of a strong hybridization with the surface Rayleigh mode of the substrate. In Sec. II, we present the dispersion curves obtained from inelastic He-scattering experiments. Section III provides the theoretical background and the results of the slab calculations. The comparison between the experimental and calculated phonon dispersion is presented in Sec. IV.

II. EXPERIMENT

The structure and phase transitions of Xe adsorbed on the Cu(110) surface are described in detail elsewhere.[8,9] Here we report on the dynamics of the Xe monolayer in the most stable structure (26×2) phase. The energy and dispersion of the Xe adlayer vibrational modes and the dynamical cou-

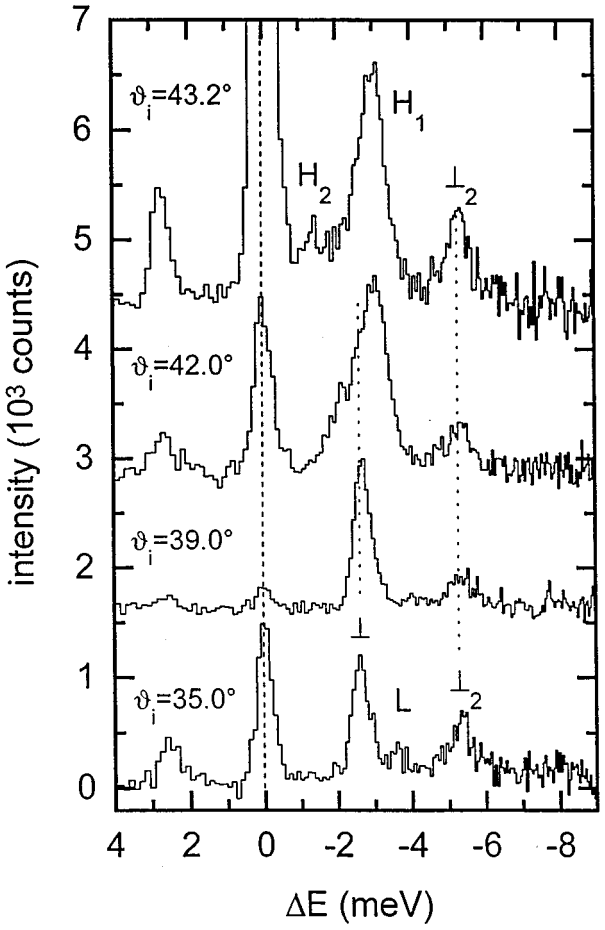

FIG. 2. He energy loss spectra recorded from the (26×2) HOC Xe monolayer on Cu(110) along the $\overline{\Gamma X}$ direction for different incident angles ϑ_i. Incident He beam energy $E_i=18.3$; the spectra were taken at $T<25$ K.

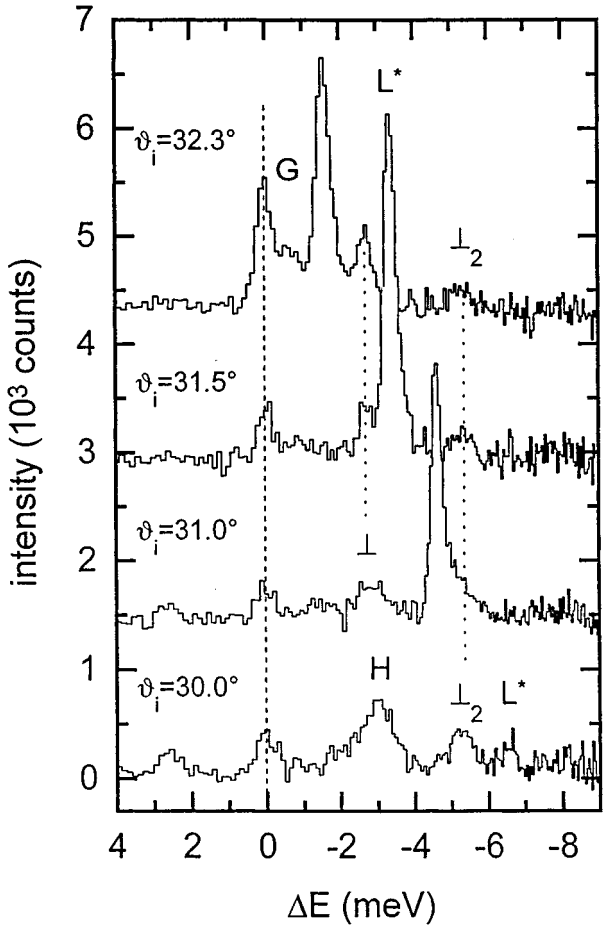

FIG. 3. He energy loss spectra recorded from the (26×2) HOC Xe monolayer on Cu(110) along the $\overline{\Gamma Y}$ direction for different incident angles ϑ_i. Incident He beam energy $E_i=18.3$; the spectra were taken at $T<25$ K.

pling to the underlying Cu(110) substrate were investigated by inelastic He scattering.

The experimental setup is described in Ref. 11. For the present experiments a He beam with an energy $E_i=18.3$ meV and an energy spread of about 0.2 meV was generated by expanding He from high pressure ($\sim$150 bar) through a liquid nitrogen cooled nozzle (5 μm diameter). The beam is scattered from the sample and detected with of a quadrupole mass spectrometer. The angular divergence of the incoming beam and the angle subtended by the detector are both 0.2°. For the present purpose an ''in-plane'' scattering geometry was used, in which the surface normal lies in the same plane as the incoming and outgoing beams. We have further limited ourselves to azimuthal orientations of the sample along either one of the $[1\bar{1}0]$ and [001] high-symmetry directions of the Cu(110) surface. In order to determine the energy transfer during the collision, a pseudorandom time-of-flight analysis is performed on the scattered He atoms before they enter the detector. Knowing the length of the flight path ($l=790$ mm) the time-of-flight distribution is readily converted into an energy spectrum. From the characteristic peaks in the energy spectrum (see Figs. 2 and 3) the single-phonon loss and gain features can be identified. The phonon dispersion curves are obtained by recording energy spectra at a different wave vector transfer Q parallel to the surface. This is achieved by rotating the sample around its polar axis, changing both the incident and outgoing angle ϑ_i and ϑ_f of the He beam with respect to the surface normal. Since the total scattering angle is fixed at 90°: $\vartheta_i+\vartheta_f=90°$. Under these conditions, the conservation of energy and parallel momentum can be used to relate the observed phonon energy $\hbar\omega$ and the corresponding parallel momentum transfer Q:

$$\hbar\omega=E_i\left[\left(\frac{\sin\vartheta_i+Q/k_i}{\cos\vartheta_i}\right)^2-1\right], \tag{1}$$

where $k_i=\sqrt{2mE_i}/\hbar$. The above expression is referred to as *scan curve*. At a particular angle of incidence ϑ_i only those phonons with Q and $\hbar\omega$ values defined through Eq. (1) can be observed experimentally.

The sample is a high-quality single crystal Cu(110) surface with a miscut angle $<0.2°$. It was cleaned *in situ* by repeated cycles of sputtering with Ar^+ ions and heating to about 1000 K. The quality was routinely checked by He diffraction, which constitutes a sensitive measure for surface defects and impurities. The base pressure in the scattering chamber was in the low 10^{-11} mbar range.

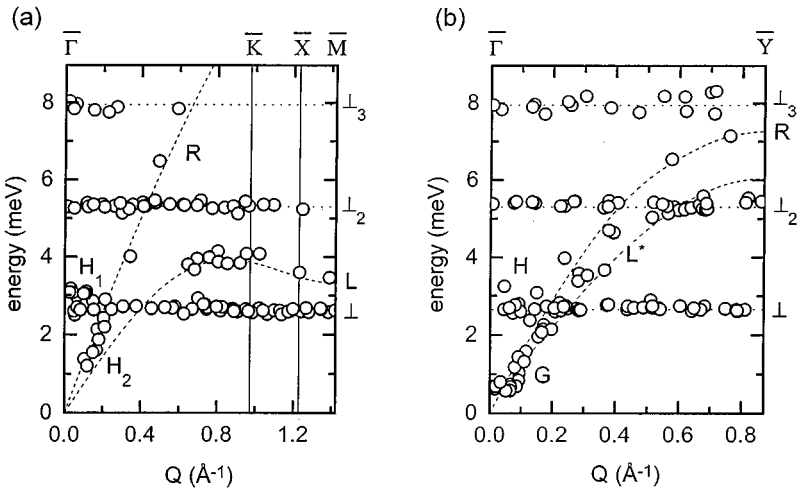

FIG. 4. Measured phonon dispersion curves (folded into the first Brillouin zone) for the (26×2) HOC Xe monolayer on Cu(110) obtained from He energy loss spectra as shown in Figs. 2 and 3 and using Eq. (1). (a) $\overline{\Gamma X}$ direction; (b) $\overline{\Gamma Y}$ direction. Dashed lines: Caculated dispersion curves using a simple two-dimensional model ignoring adlayer-substrate dynamical coupling (Sec. III A) (Ref. 12). The dispersion of the substrate Rayleigh wave is taken from Ref. 15.

The Xe monolayer was adsorbed by exposing the cold Cu(110) surface ($\leqslant$50 K) to a Xe partial pressure or by means of a doser positioned in front of the sample. The Xe coverage was controlled by monitoring the specularly reflected He intensity. Once the monolayer coverage was reached, the Xe gas was pumped off. Finally, the sample was carefully annealed at around 55 K and cooled down to about 20 K where most of the inelastic He spectra were recorded. The so prepared Xe monolayer showed a diffraction pattern characteristic of the (26×2) phase shown in Fig. 1(a).[9,12]

Time-of-flight spectra were recorded along the two high symmetry axes of the substrate, i.e., along the $[1\bar{1}0]$ and [001] directions in real space, corresponding, respectively, to the $\overline{\Gamma X}$ and $\overline{\Gamma Y}$ directions in reciprocal space [Fig. 1(c)]. Besides the diffuse elastically scattered beam ($\Delta E=0$), two phonon peaks at $\Delta E=2.6$ meV and $\Delta E=5.3$ meV can be clearly distinguished in Figs. 2 and 3. They are attributed to the single and double excitations ($\perp$ and $\perp_2$, respectively) of the perpendicular vibrational mode of the Xe overlayer.[13] The third feature at intermediate energies denoted L in the $\overline{\Gamma X}$ direction (Fig. 2) has been assigned to the longitudinal Xe phonon.[12] For smaller Q values the $\perp$ mode is split into two structures H_1 and H_2 appearing at around 3 meV and 1.6 meV in the topmost spectrum of Fig. 2. Along the $\overline{\Gamma Y}$ direction (Fig. 3), the perpendicular vibrational modes $\perp$ and $\perp_2$ are observed at the same energies as along $\overline{\Gamma X}$ with again a peak splitting or broadening of $\perp$ (H) apparent in the two lower spectra. In addition, a phonon branch labeled G is observed at low energies and another one labeled L^* starting off at around 1.6 meV in the upper spectrum and exhibiting a strong dispersion towards values above 6 meV in the spectrum at $\vartheta_i=30.0°$. As will be shown below, this mode L^*, in particular, cannot be assigned in a straightforward way to the unperturbed longitudinal Xe mode along this direction. Instead, a special coupling mechanism to the Cu(110) substrate has to be taken into account.

From a large number of spectra taken at different scattering angle we have extracted the phonon dispersion $\hbar\omega(Q)$ along $\overline{\Gamma X}$ and $\overline{\Gamma Y}$ and the results are plotted in Figs. 4(a) and 4(b), respectively. We have used a reduced zone scheme, based on the first Brillouin zone of the quasihexagonal Xe lattice [$Q(\bar{K})=0.98$ Å^{-1}, $Q(\bar{M})=1.422$ Å^{-1}, $Q(\bar{Y})=0.87$ Å^{-1}].[12] As can be seen, there is no indication for any periodicity in the dispersion curves other than due to the quasihexagonal arrangement of the Xe atoms. Indeed, a significant shortening of the Brillouin zone along the $\overline{\Gamma X}$ direction (backfolding) would be expected if Umklapp processes in the He scattering due to the (26×2) adlayer periodicity were strong enough.

Using Figs. 4(a) and 4(b), we can summarize our experimental findings on the dispersion of the Xe adlayer along the $\overline{\Gamma X}$ and $\overline{\Gamma Y}$ directions as follows: The perpendicular mode for a wave vector transfer Q$\geqslant$0.3 Å^{-1} is almost dispersionless for both directions. Along $\overline{\Gamma X}$, it exhibits for smaller Q values an avoided crossing leading to the appearance of branches H_1 and H_2. While a similar hybridization feature seems to exist also in Fig. 4(b), it is rather difficult at this stage to identify the exact nature of the mode H associated with a phonon energy of about 3 meV close to the $\bar{\Gamma}$ point. The longitudinal phonon mode L in Fig. 2 has been reported previously in Ref. 12. The dispersion of this mode has been shown to be strongly affected by the anisotropic distortion of the Xe monolayer.

The highly dispersive phonon mode labeled L^* in Figs. 3 and 4(b) has an unexpected behavior since it appears to fit, at least on a restricted range of Q values, the Rayleigh mode (R) of the clean Cu surface. This characterizes a different type of dynamical coupling phenomenon. The following question arises: how can this signal possibly be associated with the longitudinal mode of the Xe monolayer along this $\overline{\Gamma Y}$ direction and/or why are the He atoms sensitive to this substrate mode. It is the aim of this paper to give a consistent interpretation of the experimental data. In particular, we will discuss the obvious difference in the dispersion behavior along the $\overline{\Gamma X}$ and $\overline{\Gamma Y}$ directions.

III. CALCULATIONS

The interpretation of the dispersion curves for the (26×2) HOC monolayer phase requires the diagonalization of the dynamical matrix associated with the 2D unit cell of the monolayer. Its area is (66.3×7.2) Å^2 and it contains 30 Xe atoms. We use a slab model to describe the monolayer-substrate dynamics with a minimum of 40 substrate planes. This slab width of about 100 Å can be considered as a compromise between the required accuracy of the substrate dynamics and the simplicity necessary to interpret the dispersion curves. To avoid possible artefacts connected to this finite width, tests were performed using a larger number (60 and 80) of atomic planes. They do not reveal significant changes in the curves for Q values larger than 0.1 Å^{-1}, but the increasing number of dispersion curves at very small Q values lead to a much more intricate scheme. This leads us to conclude that a 40 planes slab model is quantitatively accurate for $Q\geqslant0.1$ Å^{-1} and sufficiently correct for smaller Q values to allow a qualitative discussion. Within this model, each substrate plane contains 52 Cu atoms and the dynamical equations of motion lead to a (6420×6420) square matrix which should be diagonalized for each wave vector. While, in practice, such a calculation is time consuming but tractable, it will give rise to a multifolding of the dispersion curves due to the dramatic decrease of the size of the first Brillouin zone (BZ), as compared to that of the clean (1×1) Cu(110) surface. The maximum value of the wave vector $\mathbf{Q}=(Q_x,Q_y)$ at the edge of the BZ along $\overline{\Gamma X}$, equal to 1.23 Å^{-1} for the free Cu surface, reduces to 0.094 Å^{-1} for the (26×2) structure. Such a behavior is not observed in the experiment where the data points of the longitudinal mode along $\overline{\Gamma X}$ reflect the periodicity of the quasihexagonal Xe primitive cell. It thus appears irrelevant to perform the whole calculation for the (26×2) structure and we rather consider three situations which are well suited for the interpretation of the experimental features.

A. The distorted incommensurate monolayer phase

The monolayer is assumed to be adsorbed on a rigid and strictly planar substrate, without corrugation. The adsorbate-substrate coupling is taken into account through a single force constant which describes the stiffness of the Xe atom-surface bond. The value of this force constant $\phi_{zz}=196$ meV Å^{-2} is obtained from the experimental frequency of the perpendicular monolayer mode $\omega_\perp$ as $\phi_{zz}=M\,\omega_\perp^2$; M is the Xe atomic mass and $\omega_\perp=2.6$ meV.[8,13] The Xe-Xe interactions are modeled by a Lennard-Jones potential with parameters $\epsilon=24.87$ meV and $\sigma=3.885$ Å.[14]

The hexagonal incommensurate structure of the monolayer is then distorted by varying the length of the sides of the regular lozange defining the unit cell in order to simulate the expansion of the distance between Xe atoms along dense Cu rows and its contraction along the perpendicular direction in the (26×2) phase. In this way, the dispersion of the longitudinal mode L is indeed well reproduced[12] [Fig. 4(a)]. In contrast, the model cannot explain the corresponding dispersion branch L^* along the [001] direction as apparent from Fig. 4(b). Instead of following the calculated curve characteristic of a floating monolayer, the data points lie rather close to the Rayleigh mode (R) of the bare Cu substrate. Moreover, the pronounced hybridizations leading to the curves H_1 and H_2 [Fig. 4(a)] and H and G [Fig. 4(b)] cannot be explained without including the dynamical coupling between monolayer and substrate modes.

B. The $c(2\times2)$ commensurate phase dynamically coupled to the substrate

The total number of atoms to be considered in the slab model for a $c(2\times2)$ geometry is 82 when 40 Cu planes are used to describe the substrate. Each substrate plane contains two Cu atoms and the two outer planes on both sides of the slab contain one Xe atom each.

The interactions between atoms belonging to the substrate or to the Xe adlayer are described by pairwise potentials and the components of the corresponding force constant tensor associated with the coupling between atoms i and j at a distance R_{ij} are defined by

$$\Phi_{\alpha\beta}(i,j)=-\frac{\phi'_{ij}}{R_{ij}}\delta_{\alpha\beta}+\frac{R_i^\alpha R_j^\beta}{R_{ij}^2}\left(-\phi''_{ij}+\frac{\phi'_{ij}}{R_{ij}}\right), \qquad (2)$$

where ϕ'_{ij} and ϕ''_{ij} are the first and second derivatives of the potentials. The components of the force constant tensor describing the bulk Cu substrate are expressed in terms of a single nearest neighbor force constant ϕ''_b. At the surface the force constant is modified to take into account the relaxation of the Cu(110) surface;[15] four values correspond to nearest neighbor Cu atoms located into two adjacent or two second adjacent substrate planes and four others describe the interactions between the nearest neighbor along $[1\bar{1}0]$ and the second nearest neighbor Cu atoms along [001] in the surface plane. These eight surface force constants are given, in units of ϕ''_b, in Tables I and II of Ref. 15.

The interactions between adsorbate and substrate atoms are described by pairwise shifted Morse hybrid potentials which have been shown to reproduce quite well the thermodynamic and structural properties of the monolayer.[8] In particular, the perpendicular mode frequency calculated with the best fit potential is equal to the measured value (2.6 meV). For the interactions between Xe atoms within the adsorbate layer, the Lennard-Jones potential given in Sec. III A yields appropriate values for the intralayer force constants.

The dynamical matrix for the $c(2\times2)$ structure can then be written as

$$D_{\alpha\beta}(sp,s'p',\mathbf{Q})=[M_pM_{p'}]^{-1/2}\sum_{l'}\Phi_{\alpha\beta}\begin{pmatrix}0 & l'\\ sp & s'p'\end{pmatrix}e^{i\mathbf{Q}\cdot\mathbf{R}(l')}, \qquad (3)$$

where the indices s, p, and l represent the atom number s in the lth two-dimensional unit cell of the pth plane. M_p corresponds to the Xe atomic mass for $p=1$ and 42 and to the Cu mass for $p=2,\ldots,41$. The components of the force constant tensor between atom $i=(l,s,p)$ and $j=(l',s',p')$ are given by Eq. (2) and $\mathbf{R}(l)$ defines the position of the lth 2D cell. The corresponding eigensolutions of $\underline{\mathbf{D}}$ are obtained from the dynamical equation

$$\sum_{\beta,s',p'} D_{\alpha\beta}(sp,s'p',\mathbf{Q})e_\beta(s'p',\mathbf{Q},j)=\omega_j^2(\mathbf{Q})e_\alpha(sp,\mathbf{Q},j). \tag{4}$$

ω and **e** characterize the eigenvalues and the eigenvectors associated with the jth branch ($j=1,\ldots,246$) for the wave vector **Q.**

Figures 5(a) and 5(b) display the dispersion curves $\omega_j(\mathbf{Q})$ calculated with the above model for a wave vector **Q** along the $[1\bar{1}0]$ and [001] directions, respectively. The phonon energies range between 0 and 30 meV. Above 10 meV, they correspond to nearly undistorted substrate vibrations since the dispersion scheme compares quite well to that calculated elsewhere for the bare Cu(110) substrate.[15] Note that, as shown in Fig. 1(b), the unit cell of the $c(2\times2)$ phase is twice the size of the clean substrate unit cell and thus its first Brillouin zone is half as large as the one of the pure Cu(110) surface. As a consequence the dispersion scheme of the substrate vibrations for the $c(2\times2)$ phase along the $[1\bar{1}0]$ and [001] directions is a mixture of the $\overline{\Gamma X}$, $\overline{SY}$, and $\overline{\Gamma Y}$, $\overline{SX}$ dispersion curves, respectively.[16] A direct comparison of the bulk dispersion curves of the pure Cu substrate and of the Xe covered Cu substrate thus requires us to remove the folding of the branches. After this procedure, the known scheme of the clean Cu(110) vibrational modes[17] is recovered, indicating that the Xe monolayer has no appreciable influence on the high frequency bulk modes.

By contrast, the modes below 10 meV, in general, are combined adsorbate and substrate surface vibrations and they are thus characteristic of the influence of the adsorbed monolayer on the dynamics of the whole system. For the two perpendicular directions Q_x and Q_y, the three modes ranging between 2 and 4 meV are clearly monolayer vibrations. These modes are polarized along the longitudinal (L), transverse (T), and perpendicular ($\perp$) directions with respect to the wave vector **Q**, respectively. The almost nondispersive mode at about 2.6 meV characterizes the vibrations of the Xe atoms perpendicular to the surface. The other four branches labeled L_x, T_x, L_y, and T_y are assigned to the Xe vibrations parallel to the surface plane. Along the $\overline{\Gamma X}$ direction (which corresponds to the $[1\bar{1}0]$ or x direction in real space), the force constant and thus the mode frequency is smaller than along the $\overline{\Gamma Y}$ direction ([001] or y direction), as expected from examination of the asymmetry in the values of the nearest neighbor Xe-Xe distances in the $c(2\times2)$ unit cell. Hence, the lowest energy branches around 3.3 meV are attributed to the longitudinal L_x and transverse T_y modes while the other two modes at larger energy (4.7 meV) correspond to the transverse T_x and longitudinal L_y monolayer vibrations. Note that these branches are strongly hybridized with substrate modes for $Q\leqslant0.25$ Å^{-1} and that they have a quasiacoustical behavior.

The dispersion curves intersecting the zone edge at 12 meV along the $\overline{\Gamma X}$ direction and at 7.3 meV along the $\overline{\Gamma Y}$ direction are identified as the substrate Rayleigh mode. These values are close to those obtained for the Rayleigh wave of the pure Cu(110) substrate[15] (7.2 and 12 meV, respectively). Along both directions, the Rayleigh mode exhibits avoided crossings and hybridizes with the Xe monolayer modes L and $\perp$ for $Q\leqslant0.2$ Å^{-1}. The appearance of addi-

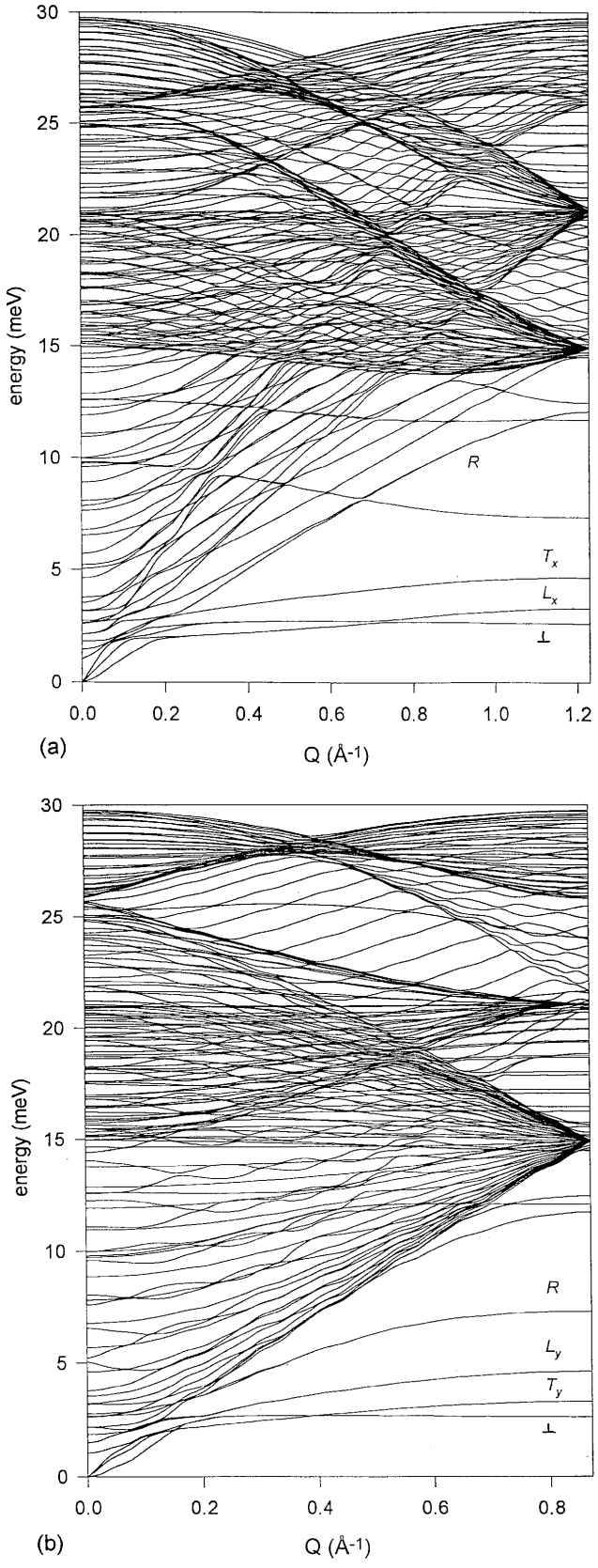

FIG. 5. Calculated dispersion curves for the $c(2\times2)$ phase of Xe adsorbed on Cu(110). Energy (meV) vs wave vector Q (Å^{-1}) along the $\overline{\Gamma X}$ direction (a) and along the $\overline{\Gamma Y}$ direction (b). L, T, and $\perp$ characterize the longitudinal, transverse, and perpendicular monolayer modes. R labels the Rayleigh mode of the substrate.

tional modes (e.g., the one which intersects the zone edge at 7.3 meV along the $\overline{\Gamma X}$ direction) is due to the already mentioned folding. They correspond, in fact, to substrate surface modes along the $\overline{SX}$ and $\overline{SY}$ directions.

C. A model for the (26×2) structure: The modified $c(2\times2)$ phase

As already mentioned, the dynamics of the (26×2) HOC phase can be approximated by considering the $c(2\times2)$ geometry and assuming that the distortion of the (26×2) geometry can be integrally taken into account through the modification of the lateral force constants between Xe atoms. Such a modification appears, in a straightforward way, through the change of the interatomic distances in the Xe-Xe potential. The new force constants are calculated from Eq. (2) by considering that the inter- and intra-row nearest neighbor Xe distances are those obtained for the HOC structure,[8] i.e., $a_{\mathrm{Xe}}=4.42$ Å and $b_{\mathrm{Xe}}=4.23$ Å, respectively. Such an approach could appear arbitrary for highly corrugated substrates, since changing the Xe-Xe distance and thus the adsorption sites for each Xe atom could introduce dramatic modifications in the atom-surface bond strength. The situation is quite different for the Cu(110) surface since it has been shown that the equilibrium troughs for the Xe atoms are flat;[8] this is indeed the main reason for the occurrence of several metastable HOC phases for this system.[8,9] Therefore, a change of the Xe-Xe distance in the monolayer will have a negligible effect on the values of the force constants between the layer and the substrate, provided that the Xe centers of mass remain confined along the troughs of the holding potential. As a result, the monolayer dynamics will be changed without concomitant influence on the substrate dynamics.

Figures 6(a) and 6(b) exhibit the dispersion curves for this distorted $c(2\times 2)$ phase along the $\overline{\Gamma X}$ and $\overline{\Gamma Y}$ directions. Only energies below 8 meV are shown because the shape of the bulk substrate modes are not modified, and they are exactly identical to the dispersion curves of the $c(2\times2)$ phase displayed in Figs. 5(a) and 5(b). In addition, we see that also the substrate Rayleigh mode and the perpendicular monolayer vibration $\perp$ are not significantly affected by these changes. In contrast, the energies of the longitudinal monolayer mode L_x and, to a lesser extent, of the transverse T_x mode increase substantially, due to the contraction of the Xe-Xe distance along $[001]$ and to the concomitant expansion along $[1\bar{1}0]$. A similar behavior is exhibited by the monolayer modes L_y and T_y along the $\overline{\Gamma Y}$ direction which are stiffened for the same reason. Two important consequences, which will be shown to be at the basis of the interpretation of the unexpected behavior of the dispersion branches in Figs. 4(a) and 4(b), result from these modifications. (i) For $Q_x\geqslant0.3$ Å^{-1}, the L_x and T_x vibrational modes now lie within an energy window above the perpendicular monolayer mode and below the substrate Rayleigh mode [Fig. 6(a)]. (ii) The longitudinal monolayer mode L_y moves closer to the Rayleigh mode of the substrate [Fig. 6(b)].

For $Q\leqslant0.3$ Å^{-1}, the dispersion curves exhibit a very intricate shape with several avoided crossings. Such a behavior cannot be analyzed in a straightforward way and it requires to study simultaneously the **Q** dependence of the eigenvalues and the eigenvectors of the dynamical matrix, i.e.,

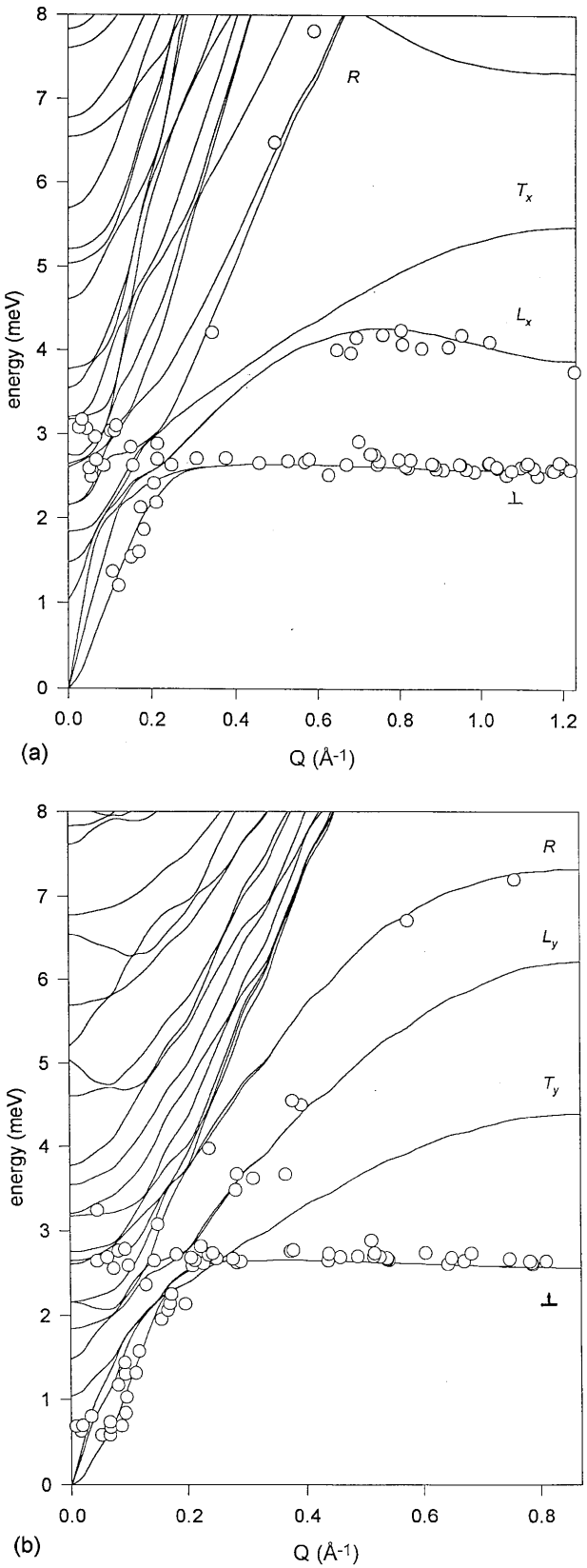

FIG. 6. Dispersion curves for the (26×2) HOC phase of Xe adsorbed on Cu(110). Energy (meV) vs Q (Å^{-1}) along the $\overline{\Gamma X}$ direction (a) and along the $\overline{\Gamma Y}$ direction (b). Full curves correspond to calculations while open circles are the experimental data. L, T, and $\perp$ characterize the longitudinal, transverse, and perpendicular monolayer modes. R labels the Rayleigh mode of the substrate.

both the vibration energies and the mode polarizations. Instead of plotting the spectral density in a separate figure, we give for each dispersion curve the step by step polarization change along the whole BZ. This is performed by calculating, for each **Q** value, the mode polarization $E_\alpha = |e_\alpha(sp,\mathbf{Q},j)|$ associated with the various dispersion curves [Eq. (4)]. Note that the components $e_\alpha(sp,\mathbf{Q},j)$ of the eigenvectors are complex quantities, hence we take the modulus of each component. It should be mentioned that the He probe is mostly sensitive to the atomic displacements in the topmost layer. We can, therefore, limit our analysis to the modes within the Xe layer, only ($p=1$ or 42). Moreover, we may disregard the transverse polarization since for in-plane scattering conditions used here the He atoms are known to probe only vibrations which lie in the saggital plane, i.e., longitudinal and perpendicular modes. We thus adopt the following procedure to eliminate unobservable transverse modes (modes along y for Q along $\overline{\Gamma X}$ and along x for Q along $\overline{\Gamma Y}$, respectively) and to quantify the longitudinal or perpendicular character of a vibration. A mode is assumed to be perpendicular or longitudinal if the corresponding component of the polarization E_z or $E_{\alpha=x \text{ or } y}$ in the Xe layer represents more than 10% of the normalized eigenvector ($E_z/E>0.1$ or $E_\alpha/E>0.1$).

In Fig. 7, only those (Q, $\hbar\omega$) values which satisfy these criteria are plotted. Thus, Fig. 7(a), corresponding to Q along $\overline{\Gamma X}$ contains only modes that are polarized along x and z. As can be seen, such various modes are present throughout the Brillouin zone. For $Q_x \geqslant 0.3$ Å^{-1}, the dispersionless mode $\perp$ is clearly perpendicular while L_x is longitudinal. The hybridization between these modes and the Rayleigh wave at small Q_x values leads to dispersion curves with partially weighted perpendicular and longitudinal polarization; such polarizations will be called *mixed*. It is also interesting to note that the mode associated with the Rayleigh wave remains visible, within our criterium, only for $Q_x \leqslant 0.4$ Å^{-1}. This mode is polarized partly longitudinal and partly perpendicular and it hybridizes with the perpendicular monolayer mode for $Q_x \approx 0.3$ Å^{-1}. As a result of the various avoided crossings at small wave vector Q_x, most of the curves around 3 meV are mixed. Note also that, close to the $\overline{\Gamma}$ point ($Q=0$), the lowest energy curve exhibits the acoustic behavior of the Rayleigh mode, with a perpendicular polarization.

Figure 7(b) shows the dispersion curves along the $\overline{\Gamma Y}$ direction. We see that, in addition to the $\perp$ and L_y monolayer modes, the Rayleigh mode is also visible throughout the entire Brillouin zone. For $Q_y \geqslant 0.2$ Å^{-1}, the dispersionless monolayer mode $\perp$ is clearly polarized in the perpendicular direction while L_y is longitudinal. Both modes hybridize with the Rayleigh wave at $Q_y \approx 0.2$ Å^{-1} and for smaller values of the wave vector Q, they are equally weighted perpendicular and longitudinal. At the same time the Rayleigh mode exhibits a very complex behavior. Initially, as a result of the hybridization with the $\perp$ mode, the polarization of the Rayleigh mode is mixed, in close analogy with the behavior displayed in Fig. 7(a). Then for $0.25 \leqslant Q_y \leqslant 0.6$ Å^{-1}, the polarization is rather longitudinal, while for $Q_y \geqslant 0.6$ Å^{-1}, it switches again to being mixed and finally, at the zone edge, the Rayleigh wave is purely perpendicularly polarized. At first, it appears surprising that the Rayleigh mode could be

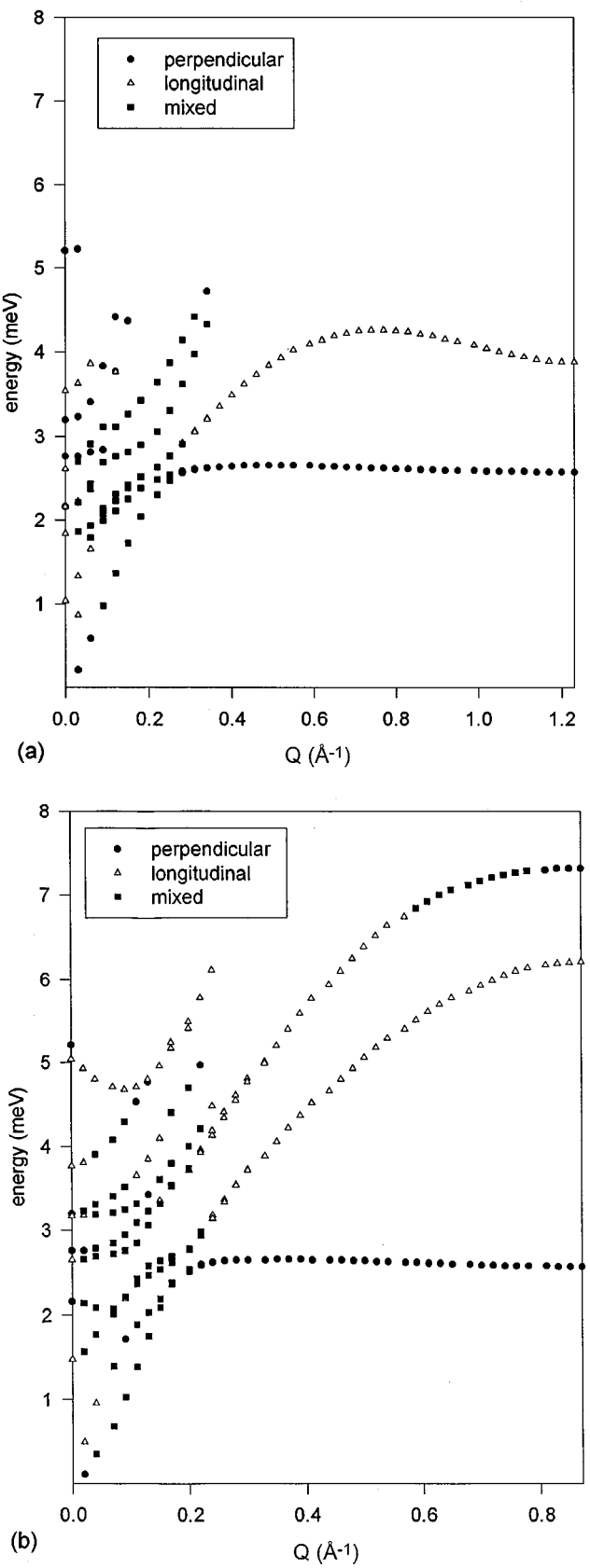

FIG. 7. Calculated dispersion curves with the corresponding mode polarization for the (26×2) HOC phase. Energy (meV) vs Q (Å^{-1}) along the $\overline{\Gamma X}$ direction (a) and along the $\overline{\Gamma Y}$ direction (b). Circles, triangles, and squares characterize modes with mainly perpendicular, longitudinal, and mixed polarization, respectively.

perpendicularly polarized at the $\bar{Y}$ point. Indeed, for the bare Cu(110) surface, the Rayleigh mode along the $\bar{\Gamma}\bar{Y}$ direction is strongly softened and polarized along the longitudinal direction, as a result of the substrate anisotropy.[15] For the Xe covered Cu surface, the presence of the monolayer does not appreciably modify its frequency behavior but seems to change its polarization drastically. The explanation, however, is quite simple and intuitive. An analysis of the vibration pattern of the Rayleigh mode close to the $\bar{Y}$ point for the clean Cu(110) surface reveals that the atoms in successive layers are alternatingly displaced parallel and perpendicular with respect to the surface plane. In fact, the sequence is exactly preserved after the adsorption of the Xe monolayer. The Xe layer adopts the ''correct'' phase in this sequence, i.e., it is polarized perpendicularly on top of the first (longitudinally polarized) Cu surface layer. Between 3 and 5 meV and for $Q_y \leqslant 0.2$ Å^{-1}, there are some additional curves which characterize mostly perpendicular surface vibrations. Finally, it should be mentioned that the lowest energy phonons for $Q_y \approx 0$ correspond to perpendicular vibrations.

IV. COMPARISON BETWEEN CALCULATIONS AND EXPERIMENTS.

The experimental data points displayed in Figs. 4(a) and 4(b) are plotted together with the calculated dispersion curves in Figs. 6(a) and 6(b), respectively. This allows a direct comparison with the calculated dispersion curves without obscuring the readability of Figs. 7(a) and 7(b) to which they should be compared as far as their polarization is concerned. If we disregard the two and three phonon excitations of the perpendicular monolayer mode at about 5.3 and 7.9 meV which are not considered in our calculations, three main modes can be distinguished in Figs. 6(a) and 6(b) which correspond to H or G, L and $\perp$ according to the nomenclature in Fig. 4.

In Fig. 6(a), for $Q_x \geqslant 0.3$ Å^{-1}, two sets of points can be distinguished, labeled $\perp$ and L in Fig. 4(a). The dispersionless mode at 2.6 meV ($\perp$) can be clearly assigned to the purely perpendicular vibration in Fig. 7(a), since it is the only mode which appears in this energy range. The experimental points, labeled L in Fig. 4(a), which occur at higher energies, can be assigned to the purely longitudinal monolayer mode L_x in the calculated dispersion scheme [Figs. 6(a) and 7(a)]. Note that the shape of the curve can be interpreted as the result of the properties of the (26×2) geometry. Indeed, the energy maximum which occurs for $Q_x \approx 0.8$ Å^{-1} does not appear for the $c(2\times 2)$ structure. The fact that this mode is observed experimentally is rather unexpected[12] since it is generally assumed that He atoms are mainly sensitive to perpendicular vibrations. It may be noted that the Rayleigh mode of the substrate lies far apart from the longitudinal L_x mode and therefore we do not expect a strong coupling between these two branches. The observation of a purely longitudinally polarized mode is consistent with recent conclusions drawn from inelastic He scattering experiments on clean Cu(100) and Ag(100) surfaces.[18]

At smaller Q_x values, $0.1 \leqslant Q_x \leqslant 0.25$ Å^{-1}, some experimental points in Fig. 4(a) either follow a behavior along a straight line around 2.6 meV (H_1) or dramatically decrease in energy with decreasing Q (H_2). This is interpreted by means of Figs. 6(a) and 7(a) as the result of a set of hybridized dispersion curves implying mainly the Rayleigh mode and the $\perp$ and L_x monolayer modes. No mode is purely perpendicular or longitudinal, all are mixed. While points H_2 are clearly due to hybridization between the Rayleigh mode and the perpendicular monolayer mode, points H_1 may also include avoided crossings between the substrate modes (Rayleigh plus other modes) and the L_x and $\perp$ vibrations, yielding curves in the energy range between 2.5 – 3.5 meV.

Near the $\bar{\Gamma}$ point ($Q_x \rightarrow 0$), the effect of the hybridization is reduced and the modes tend to recover their polarization specificity. The acoustic mode as well as the modes around 2.6 meV and 3.2 meV become perpendicular. In contrast, the vibrations around 1 and 3.5 meV recover their longitudinal polarization. These latter modes cannot be observed since they lie in a region with dominant perpendicular vibrational modes.

A similar scheme for the data points is obtained along the $\bar{\Gamma}\bar{Y}$ direction in Fig. 6(b). For $Q_y \geqslant 0.25$ Å^{-1}, two sets of points [$\perp$ and L^* in Fig. 4(b)] can be distinguished. The experimental points at 2.6 meV correspond to the dispersionless perpendicular monolayer mode $\perp$ [Fig. 7(b)]. The most striking feature is observed for the other set of points L^*, when compared to the dispersion curves along the perpendicular direction $\bar{\Gamma}\bar{X}$. In fact, L^* fits quite well the longitudinal monolayer mode [L_y in Fig. 6(b)] up to $Q_y = 0.4$ Å^{-1} but then it tends to follow the substrate Rayleigh mode (R) for $0.5 \leqslant Q_y \leqslant 0.87$ Å^{-1}. An understanding of such a feature is given by the examination of the polarization of L_y and the Rayleigh mode in Fig. 7(b). Indeed, as Q_y increases from 0.3 Å^{-1}, L_y recovers its purely longitudinal polarization, whereas the Rayleigh mode polarization becomes mixed for $0.6 \leqslant Q_y \leqslant 0.8$ Å^{-1} and then perpendicular at the edge of the BZ. There is thus a large Q_y region for which (i) the two modes R and L_y are clearly longitudinal and (ii) the two modes are roughly parallel and close in energy. Since no other phonons lie within this region, we expect to observe both the longitudinally polarized L_y and Rayleigh modes. However, the assignment of the measured inelastic signal to one of these two vibrations is difficult due to experimental resolution. At larger Q_y values, the L_y mode remains longitudinal while the Rayleigh mode becomes perpendicularly polarized. As a consequence, since the He probe is more sensitive to perpendicular vibrations, we observe a signal associated to the Rayleigh mode when moving towards the edge of the BZ.

For intermediate Q_y values, $0.1 \leqslant Q_y \leqslant 0.3$ Å^{-1}, both the longitudinal L_y and the $\perp$ monolayer mode hybridize with the Rayleigh wave and give rise to a set of curves polarized partly longitudinally and partly perpendicularly [Fig. 7(b)]. These mixed modes [labeled H and G in Fig. 4(b)] can therefore be detected with He scattering. The branch G results from the hybridization between the $\perp$ and L_y monolayer modes with the Rayleigh wave. The set H of points between 2.6 and 3.2 meV, in addition, contains contributions from the hybridization (overlap) of the perpendicular mode $\perp$ with other substrate modes.

Near the $\bar{\Gamma}$ point ($Q_y \leqslant 0.1$ Å^{-1}), the experiment reveals a frequency gap of about 0.7 meV which can be attributed to the frustrated translation of the adlayer parallel to the

Cu(110) surface along the $\overline{\Gamma Y}$ direction. It is not clear whether this frustrated translation can be well described within the present slab model since it crucially depends on the correct Xe-Cu potential corrugation energy. In addition, care must be taken in the interpretation of the dispersion curves at very low values ($Q \leqslant 0.1$ Å^{-1}) because of the error introduced by the finite width of the slab. Nevertheless, comparing the gap frequency of 0.7 meV with the lowest longitudinal excitation in the calculation close to the $\overline{\Gamma}$ point of about 0.5 – 1 meV [Figs. 6(a) and 7(a)] yields a rather satisfying result.

V. CONCLUSION

In this paper, we have investigated the dispersion curves of the stable (26×2) high-order commensurate Xe monolayer on Cu(110). The experimental data exhibit a characteristic behavior regarding the influence of the substrate anisotropy on the phonon mode dispersion. In particular, the occurrence of avoided crossings implying modes with a high density of states and the couplings between adlayer and substrate modes warrant a detailed analysis of the dispersion curves and of the corresponding polarizations.

The low-order commensurate $c(2\times2)$ Xe phase, although easy and convenient to model, has appeared too far from the physical reality to conduct accurate calculations on the coupled monolayer/substrate dynamics. On the other hand, the HOC (26×2) structure which is the stable structure at low temperature leads to a BZ folding which complicates the interpretation of the dispersion curves when compared to the clean Cu(110) substrate. In order to reconcile experimental dispersion curves which do not evidence backfolding and the theoretical calculations obtained for the multifolded zone associated with the (26×2) structure, we have developed an intermediate model, relying on the $c(2\times2)$ unit cell with the force constants adapted to the (26×2) structure. By doing this, we have been able to give an accurate interpretation of most of the experimental features in the inelastic He-scattering spectrum. The most interesting result has been to show that polarization exchange can occur when two dispersion curves run close to each other without necessary intersecting. This type of dynamical coupling is observed between the Xe longitudinal mode and the Rayleigh wave along the $\overline{\Gamma Y}$ direction. As a consequence, the hybridized Rayleigh wave is *longitudinally* polarized at intermediate wave vector Q but becomes strictly *perpendicular* at the zone boundary. This explains why this mode can be observed in the He-scattering experiment. In addition, the present results corroborate the usually known rule that the modes perpendicular to the surface give rise to the most intense peak in the scattering spectrum. They also show that, nevertheless, longitudinal modes connected to the monolayer or to the substrate surface can lead to observable signals provided that they lie in an appropriate energy window, namely, a region free of perpendicularly polarized modes.

ACKNOWLEDGMENTS

The authors would like to thank Dr. E. Preuß for fruitful discussions on the slab program. This work was supported by the Deutscher Akademischer Austauschdienst (DAAD) and the Ministère des Affaires Etrangères (MAE) through the PROCOPE program.

*Corresponding author. Fax number: (+33) 81666475. Electronic address: cgirardet@univ-fcomte.fr

[1] W. Kress and F.W. de Wette, *Surface Phonons* (Springer, Berlin, 1991).

[2] E. Hulpke, *Helium Atom Scattering from Surfaces* (Springer, Berlin, 1992).

[3] G. Vidali, G. Ihm, H.Y. Kim, and M.W. Cole, Surf. Sci. Rep. **12**, 133 (1991); V. Bortolani, N.H. March, and M.P. Tosi, *Interaction of Atoms and Molecules with Solid Surfaces* (Plenum, New York, 1990).

[4] B. Hall, D.L. Mills, and J.E. Black, Phys. Rev. B **32** , 4932 (1985).

[5] E. de Rouffignac, G.P. Alldredge, and F.W. de Wette, Phys. Rev. B **24**, 6050 (1981).

[6] C. Girardet and P.M.N Hoang, Surf. Sci. **282**, 288 (1993).

[7] S. Picaud, P.N.M. Hoang, and C. Girardet, Surf. Sci. **322**, 381 (1994); C. Girardet, C. Ramseyer, S. Picaud, and P.N.M Hoang, Phys. Rev. B **52**, 2144 (1995).

[8] C. Ramseyer, C. Girardet, P. Zeppenfeld, J. Goerge, M. Büchel, and G. Comsa, Surf. Sci. **313**, 251 (1994).

[9] P. Zeppenfeld, J. Goerge, M. Büchel, G. Comsa, C. Ramseyer, and C. Girardet, Surf. Sci. **366**, 1 (1996).

[10] A. Glachant, M. Jaubert, M. Bienfait, and G. Boato, Surf. Sci. **115**, 219 (1981); W. Berndt, *ibid.* **219**, 161 (1989).

[11] R. David, K. Kern, P. Zeppenfeld, and G. Comsa, Rev. Sci. Instrum. **57**, 2771 (1986).

[12] P. Zeppenfeld, M. Büchel, R. David, G. Comsa, C. Ramseyer, and C. Girardet, Phys. Rev. B **50**, 14 667 (1994).

[13] The value of 2.6 meV for the perpendicular vibration frequency is slightly larger than the 2.5 meV found in our previous study (Ref. 12). The origin of this small but systematic deviation is not known.

[14] R.J. Bell and I.J. Zucker, in *Rare Gas Solids*, edited by M.L. Klein and J.A. Venables (Academic, London, 1976), Vol. 1, p. 122.

[15] P. Zeppenfeld, K. Kern, R. David, K. Kuhnke, and G. Comsa, Phys. Rev. B **38**, 12 329 (1988).

[16] For instance, by elementary translational operations, one can show that the $\overline{S}$ point in the BZ of the clean substrate is equivalent to the $\overline{\Gamma}$ point in the $c(2\times2)$ reciprocal space.

[17] R.E. Allen, G.P. Alldredge and F. W. de Wette, Phys. Rev. B **4**, 1648 (1971).

[18] G. Benedek, J. Ellis, N.S. Luo, A. Reichmuth, P. Rugerone, and J.P. Toennies, Phys. Rev. B **48**, 4917 (1993); N. Bunjes, N.S. Luo, P. Ruggerone, J.P. Toennies, and G. Witte, *ibid.* **50**, 8897 (1994).